RSC Advances

PAPER

View Article Online
View Journal | View Issue

Cite this: *RSC Adv.*, 2014, **4**, 30798

Highly enhanced photocatalytic properties of ZnS nanowires–graphene nanocomposites

Jian Cao,*[a] Qianyu Liu,[a] Donglai Han,[bc] Shuo Yang,[bc] Jinghai Yang,*[a] Tingting Wang[a] and Haifeng Niu[a]

Received 6th May 2014
Accepted 4th July 2014

DOI: 10.1039/c4ra04164j

www.rsc.org/advances

ZnS nanowires (NWs)–graphene (GR) nanocomposites were successfully synthesized *via* an easy electrostatic self-assembly method. The results showed that ZnS NWs were well dispersed on the surface of the graphene nanosheets, forming ZnS–GR nanocomposites. The photoluminescence intensity of the ZnS–GR nanocomposites exhibited a clear quenching in comparison with that of the ZnS NWs. The ZnS–GR nanocomposites were used as photocatalysts for the degradation of methylene blue (MB) under UV light irradiation. After irradiation for 1 h, the degradation efficiency was 21.69% for ZnS NWs, 31.52% for ZnS–0.5 wt% GR, 58.69% for ZnS–3 wt% GR, 88.33% for ZnS–5 wt% GR and 80.74% for ZnS–7 wt% GR, indicating that ZnS–5 wt% GR nanocomposites had the highest photocatalytic activity. The kinetic rate constant of the ZnS–5 wt% GR nanocomposites was about 16 times higher than that of the ZnS NWs. The mechanism of the highly enhanced photocatalytic properties was attributed to the efficient separation of the photogenerated electron–hole pairs and the high specific surface area of graphene.

Introduction

Recently, graphene (GR)-semiconductor nanocomposites have attracted widespread attention due to their encouraging performance in the field of photocatalysis, which is one of the prospective ways to deal with pollutants by using solar energy.[1–6] Graphene, as a new class of two-dimensional (2D) carbon material with a thickness of one atom, possesses excellent transparency (~97.7%),[7] superior mobility of charge carriers at room temperature (~10000 $cm^2\ V^{-1}\ s^{-1}$)[8] and relatively large surface area (~2600 $m^2\ g^{-1}$),[9] making it a promising supporting matrix for photocatalysts. Various semiconductor photocatalysts such as ZnO, CdS, ZnS have been widely studied to carry out chemical reactions under light irradiation.[10–13] Among them, zinc sulfide (ZnS) is an important wide band gap ($E_g = 3.6$ eV at 300 K) semiconductor, which is considered important for applications such as ultraviolet-light-emitting diodes, electroluminescent devices, flat-panel displays, infrared (IR) windows, sensors, solar cells and so forth.[14] In addition, ZnS nanocrystals are good photocatalyst because of the rapid generation of electron–hole pairs by photo-excitation and the highly negative reduction potentials of the excited electrons.[15] However, the quick recombination of the photogenerated electrons and holes limits its photocatalytic property and decreases its photocatalytic efficiency. To date, numerous studies have demonstrated that assembling ZnS on GR can exhibit excellent photocatalytic performance.[16–18] The enhanced photocatalytic property is usually ascribed to the fact that GR can improve the transfer of the photogenerated charges from the photocatalyst surface to graphene, increase the separation efficiency of the photogenerated electron–hole pairs, and thus increase the photocatalytic efficiency.[19,20]

To extend the application of photocatalyst, GR-one dimensional (1D) semiconductor nanocomposites have been extensively investigated because of their proven potential use as the next-generation building blocks for photocatalysis due to the special morphology and efficient light-induced charge separation and transport.[21–23] Because 1D semiconductor materials (*e.g.* nanowires, nanorods, nanotubes) have large surface-to-volume ratios, direct electrical pathways for rapid transport of the photogenerated carriers and the enhanced light absorption and scattering, leading to the enhanced photocatalytic activity.[24–26] In the present work, ZnS nanowires (NWs)–GR nanocomposites were successfully synthesized *via* an easy electrostatic self-assembly method, and their photocatalytic degradation of methylene blue (MB) under UV light irradiation were investigated. The effect of the GR contents in the ZnS–GR nanocomposites on the photocatalytic property was also investigated. It is expected that integration of 2D GR and 1D ZnS NWs could yield superior electronic, optoelectronic and photocatalytic properties compared to ZnS NWs.

[a]*Key Laboratory of Functional Materials Physics and Chemistry of the Ministry of Education, Jilin Normal University, Siping 136000, P. R. China. E-mail: jhyang1@jlnu.edu.cn; caojian_928@163.com; Fax: +86 434 3294566; Tel: +86 434 3290009*

[b]*Changchun Institute of Optics, Fine Mechanics and Physics, Chinese Academy of Sciences, Changchun 130033, P. R. China*

[c]*University of Chinese Academy of Sciences, Beijing 100049, P. R. China*

Experimental section

Materials

Zinc nitrate, thiourea, ethylenediamine (EN), graphite, sodium nitrate, sulphuric acid, potassium permanganate, hydrogen peroxide, hydrochloric acid are all analytical grade (Shanghai Chemical Reagents Co.), and used without further purification.

Preparation of graphene oxide (GO)

GO was prepared by a modified Hummers' method from flake graphite. Briefly, 5 g of graphite were mixed with 5 g of $NaNO_3$ and 100 mL of H_2SO_4 under stirring for 1 h at 80 °C, and then the mixture was cooled to 0 °C in an ice bath. Then, 10 g of $KMnO_4$ were added slowly into the above mixture under stirring maintaining the temperature below 5 °C. The cooling bath was then removed and the mixture was stirred at 35 °C vigorously for 4 h. After that, 1000 mL of deionized water were added, and the temperature was increased to 98 °C and kept there for 30 min. Then, 30 mL of 30% H_2O_2 were added slowly till the color turned from brown to bright yellow. Finally, the as-prepared GO were washed alternately with 30% HCl and deionized water until pH = 7, then dried at 60 °C for 24 h.

Preparation of ZnS NWs

In a typical process, 1 mmol of zinc nitrate were dissolved in 16 mL EN and water (1 : 1 in volume ratio). After stirring for 1 h, 3 mmol of thiourea were put into the resulting complex. After stirring for 2 h, the colloid solution was transferred into a 20 mL Teflon-lined autoclave and kept at 180 °C for 12 h. After the reaction, the autoclave was taken out and cooled down to room temperature. The product was washed with ethanol and deionized water for several times and separated by centrifugation, and then dried at 60 °C for 1.5 h to get the powder.

Preparation of ZnS–GR nanocomposites

ZnS–GR nanocomposites were prepared by the electrostatic self-assembly method.[3] 0.2 g of ZnS were dispersed in 100 mL of deionized water by ultrasound for 10 min (solution A). Meanwhile, different amounts (0.001, 0.006, 0.01 and 0.014 g) of GO were added into 20 mL of deionized water by ultrasound for 1 h, respectively (solution B). Solution B was added to solution A drop by drop under vigorous stirring for 1 h. After that, the mixture was centrifuged and dispersed in 80 mL of deionized water. After stirring for 30 min, the solution was transferred into a 100 mL Teflon-lined autoclave and kept at 140 °C for 12 h. After the reaction, the autoclave was taken out and cooled down to room temperature. The product was washed with ethanol and deionized water for several times and separated by centrifugation, and then dried at 60 °C for 2 h to get the powder.

Characterization of products

X-ray diffraction (XRD) pattern was collected on a MAC Science MXP-18 X-ray diffractometer using a Cu target radiation source. Transmission electron micrographs (TEM), high-resolution transmission electron microscopy (HRTEM) and energy dispersive X-ray spectrum (EDX) images were taken on JEM-2100 electron microscope. The specimen was prepared by depositing a drop of the dilute solution of the sample in ethanol on a carbon-coated copper grid and drying at room temperature. EDAX (energy dispersive analysis of X-rays) microanalysis was performed at the SEM magnification. Raman spectrum was recorded on a Renishaw Micro-Raman spectrometer with a 514.5 nm Ar^+ ion laser as excitation. Fourier transform infrared (FTIR) spectrum was recorded on a Bruker Vertex 70 spectrophotometer in KBr pellets. X-ray photoelectron spectrum measurement was performed on a Vgescalab MK II X-ray photoelectron spectrometer (XPS) using Mg Kα radiation ($h\nu$ = 1253.6 eV) with a resolution of 1.0 eV. Photoluminescence (PL) measurement was carried out at room temperature, using 325 nm as the excitation wavelength, He–Cd Laser as the source of excitation. The samples used for the XRD, EDAX, FTIR, PL measurements were solid power.

Photocatalytic activity measurement

The photocatalytic activity of the samples was evaluated by the degradation of methylene blue (MB) in water under UV light irradiation. In a typical experiment, 10 mg of photocatalyst (ZnS NWs, ZnS–0.5 wt% GR, ZnS–3 wt% GR, ZnS–5 wt% GR and ZnS–7 wt% GR nanocomposites) were added to 50 mL MB with a concentration of 10 mg L^{-1}, and then magnetically stirred in the dark to reach the adsorption equilibrium. Subsequently, the mixture was exposed to UV light irradiation with a wavelength centered at 365 nm by a high-pressure Hg lamp (300 W) at room temperature. At a given irradiation time intervals, 4 mL of the suspension were taken out and centrifuged to remove the photocatalysts. The degraded solutions were analyzed using the UV-vis spectrophotometer (UV-5800 PC) and the characteristic absorption peak of the MB solution was monitored.

The degradation efficiency of the photocatalyst can be defined as follows:[27]

$$\text{Degradation (\%)} = (1 - C/C_0) \times 100\%$$

where C_0 is the initial concentration of MB and C is the residual concentration of MB at different illumination intervals.

The photodegradation of MB follows pseudo-first-order kinetics, which can be expressed as follows:[27]

$$\ln(C/C_0) = kt$$

where k (min^{-1}) is the degradation rate constant.

Results and discussion

The XRD patterns of the GO, GR, ZnS and ZnS–GR nanocomposites are shown in Fig. 1. The feature (001) diffraction peak of the GO (Fig. 1a) appears at 10.3° with the interplanar spacing of 0.85 nm, which is much larger than that of the natural graphite (0.335 nm),[28–30] indicating the complete oxidation of the starting graphite.[31] For the GR (Fig. 1a) obtained from the hydrothermal reduction, the diffraction peak at 10.3° disappears and a broad (002) diffraction peak of

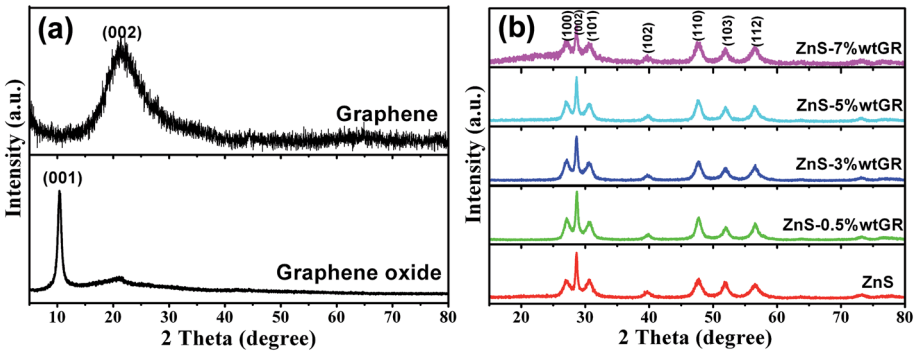

Fig. 1 XRD patterns of (a) graphene oxide and graphene; (b) ZnS and ZnS–GR nanocomposites.

graphene at 21.5° appears, which means that almost all of the GO have been transformed to GR. All the diffraction peaks for the ZnS and ZnS–GR nanocomposites (Fig. 1b) can be well indexed as the hexagonal wurtzite phase structure, which are consistent with the standard card (JCPDS no. 36-1450). Note that the (002) diffraction peak is stronger and narrower than the other peaks, suggesting a preferential growth direction along the *c*-axis. Little difference among the diffraction peaks of ZnS and ZnS–GR nanocomposites also suggests that the presence of GR does not influence the crystal nature of ZnS. Notably, a small characteristic diffraction peak of the graphene (002) can be detected in the ZnS–7 wt% GR nanocomposites (Fig. 1b magenta line). It may be due to the low amount of GR and relatively low diffraction intensity of GR in the nanocomposites of ZnS–GR.

To further obtain the microscopic morphology and structural information, the TEM and HRTEM analysis of GR, ZnS and ZnS–GR were performed (Fig. 2 and Fig. 3). The wrinkled paper-like structure of the 2D graphene sheet can be clearly seen in Fig. 2a. The HRTEM image (Fig. 2b) of the wrinkled part taken from the area marked by the red rectangle in Fig. 2a shows that there are approximately 13 layers of graphene. The TEM image of the ZnS NWs (Fig. 2c) shows that these NWs are smooth and uniform over their entire lengths and the diameter is in the range of 4–13 nm (average 7.96 nm). The HRTEM image (Fig. 2d) shows a highly crystalline NWs grown along the (002) direction. The measured (002) lattice distances of the ZnS NWs are separated by a distance of about 3.1 Å, which is close to the lattice spacing of the wurtzite ZnS (002) plane.[32] Considering our XRD study and close observation of the SAED images (Fig. 2e), it can be concluded that the diffraction rings represent the wurtzite ZnS structure. The compositional analysis of the ZnS NWs by EDAX shown in Fig. 2f demonstrates that the sample contains Zn and S element, and the amount of Zn : S is about 1 : 1.

Fig. 3 show the TEM, HRTEM and EDX images of the ZnS–0.5 wt% GR and ZnS–5 wt% GR nanocomposites. It can be seen that ZnS NWs are well dispersed on the surface of the wrinkled graphene (Fig. 3a and c). The graphene plays an important role in assisting ZnS NWs dispersion on its surface, while ZnS helps to prevent the aggregation of graphene. From Fig. 3b, the lattice of both graphene and ZnS are found, which indicates the intimate interfacial contact between graphene and ZnS NWs. Since that the transfer process of charge carriers in graphene–ZnS NWs nanocomposites is related to the interfacial interaction between graphene and ZnS NWs. It could be expected that there would be a good charge transfer during the photocatalysis process. The FFT image in the inset of Fig. 3b indicates that the ZnS–0.5 wt% GR nanocomposites possess a polycrystal-line structure, which again proves the formation of ZnS–GR nanocomposites. The growth direction of the ZnS NWs in the ZnS–5 wt% GR nanocomposites is perpendicular to the lattice fringes and the *d* spacing of the (002) plane is about 3.1 Å (Fig. 3d), which is close to the lattice spacing of the wurtzite ZnS (002) plane.[32] Its corresponding FFT image (see inset image of Fig. 3d) further confirms that it has the growth direction of (002). Elongation of the FFT spots along the growth axis indicates the presence of defects. On the basis of the EDX analysis (Fig. 3e and f), the sample contains Zn, S and C element and the amount of C in the ZnS–5 wt% GR nanocomposites (Fig. 3f) is larger than that in the ZnS–0.5 wt% GR nanocomposites (Fig. 3e).

Fig. 4 show the Raman spectra of GO and ZnS–5 wt% GR nanocomposites. All Raman spectra show similar G (the presence of sp^2 carbon-type structures) and D (the presence of defects in the hexagonal graphitic layers) band structures of carbon.[33,34] The intensity ratio of the D and G band ($I_D : I_G$) is a measure of the relative concentration of local defects or disorders (particularly the sp^3-hybridized defects) compared to the sp^2-hybridized GR domains.[35,36] It can be seen that the $I_D : I_G$ ratio is 1.01 for GO. After the hydrothermal reaction, the $I_D : I_G$ ratio is decreased to 0.78, thus indicating more graphitization of the ZnS–5 wt% GR nanocomposites resulting from the hydrothermal reduction process.[18]

Fig. 5 show the FTIR spectra of GO and ZnS–5 wt% GR nanocomposites. The characteristic peaks of GO at 1720, 1570, 1213, 1050 cm^{-1} are attributed to the C=O stretching vibrations of the –COOH groups, the C–C skeletal vibration, the C–O deformation of the C–OH groups and C–O–C stretching vibrations, respectively.[37–39] For ZnS–5 wt% GR nanocomposites, the GO related stretching bands of C–O and carboxyl groups are not observed, and the peaks at 1632 and 1086 cm^{-1} corresponding to the functional groups of stretching vibration of C=O and alkoxy C–O stretching[40,41] still remain after reduction, which is beneficial to improve the dispersion of the composites in water

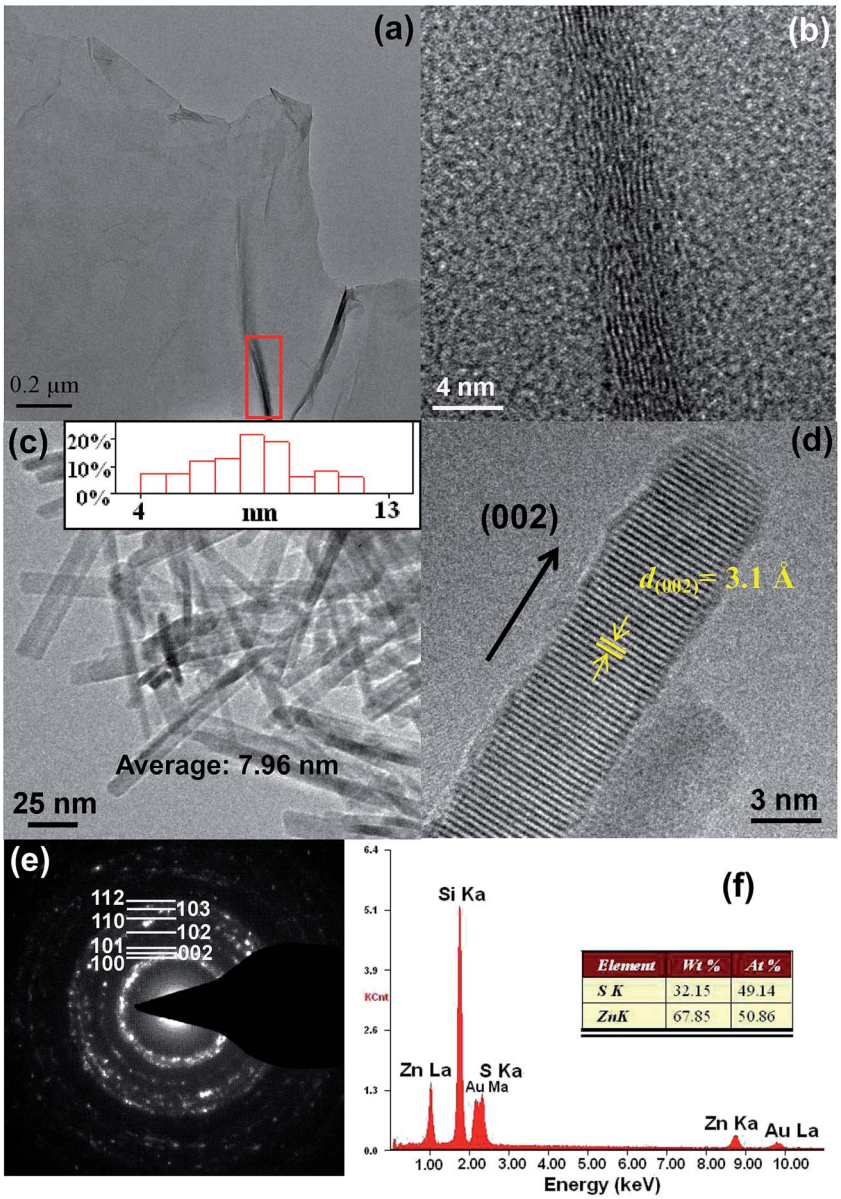

Fig. 2 (a) and (b) TEM and HRTEM images of graphene; (c) and (d) TEM and HRTEM images of ZnS NWs, the inset figure of (c) is the size distribution histogram of the NWs obtained from counting 100 NWs; (e) and (f) SAED and EDAX images of ZnS NWs.

and the stability of ZnS–GR nanocomposites. In addition, the wide band at 3427 cm^{-1} can be assigned to the absorption water or O–H groups.[42]

To analyze the chemical composition of the prepared samples and to identify the chemical state of Zn and S element in the nanocomposites, XPS analysis was carried out. Fig. 6a show the survey spectra of GO and ZnS–5 wt% GR nanocomposites, confirming the presence of C 1s, Zn 2p, S 2p and O 1s. As can be seen from Fig. 6b, the high-resolution XPS spectrum of C 1s of GO can be divided into three peaks, which correspond to the following functional groups: C–C (284.4 eV, sp^2 C atom), C–OH (285.5 eV) and O–C=O (288.4 eV, carboxyl).[17,43,44] In comparison, the high-resolution XPS spectrum of C 1s of ZnS–5 wt% GR nanocomposites can be seen in Fig. 6c. The peaks for C–OH and O–C=O still exist but much lower than that in GO, indicating that most oxygen-containing functional groups are efficiently removed from ZnS–5 wt% GR nanocomposites. This also suggest that GO have been reduced to GR. The high-resolution XPS spectrum of the Zn and S element in Fig. 6d and e shows the peak at 1022.0 and 161.5 eV, respectively, which correspond to the Zn 2p3/2 and S 2p3/2 peak of ZnS,[45,46] demonstrating that Zn and S exist in the form of ±2 valence state.

Fig. 7 present the room temperature photoluminescence (PL) spectra of ZnS NWs, ZnS–0.5 wt% GR and ZnS–5 wt% GR nanocomposites. The PL spectrum of ZnS NWs (red line) is asymmetric, which can be decomposed into six Gaussian peaks centered at 400, 422, 447, 492, 538 and 541 nm, respectively.

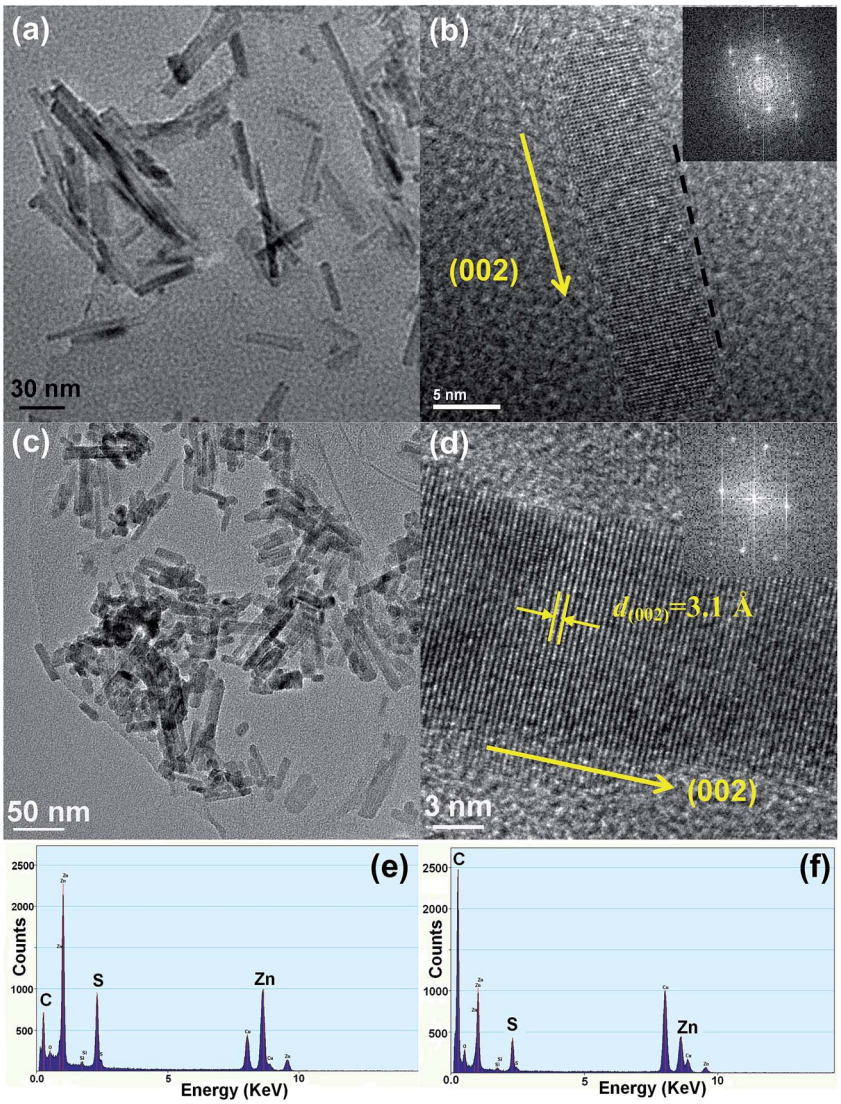

Fig. 3 (a) and (b) TEM and HRTEM images of the ZnS–0.5 wt% GR nanocomposites; (c) and (d) TEM and HRTEM images of the ZnS–5 wt% GR nanocomposites; (e) and (f) EDX images of the ZnS–0.5 wt% GR and ZnS–5 wt% GR nanocomposites.

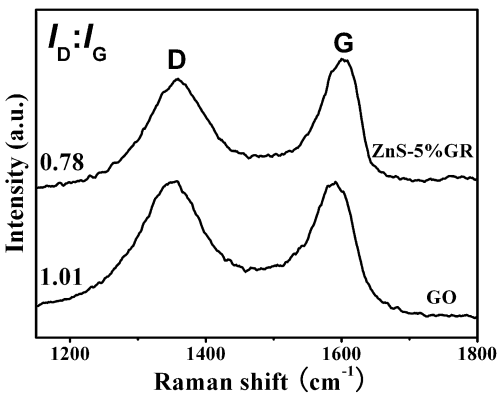

Fig. 4 Raman spectra of GO and ZnS–5 wt% GR nanocomposites.

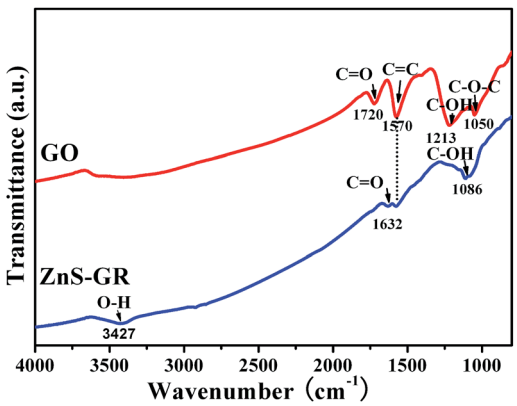

Fig. 5 FTIR spectra of the GO (red line) and ZnS–5 wt% GR nanocomposites (blue line).

According to the energy diagram of the defects distributed in ZnS, the emission peaks can be attributed to the following origins: 400 nm to the sulfur vacancy and interstitial sulfur

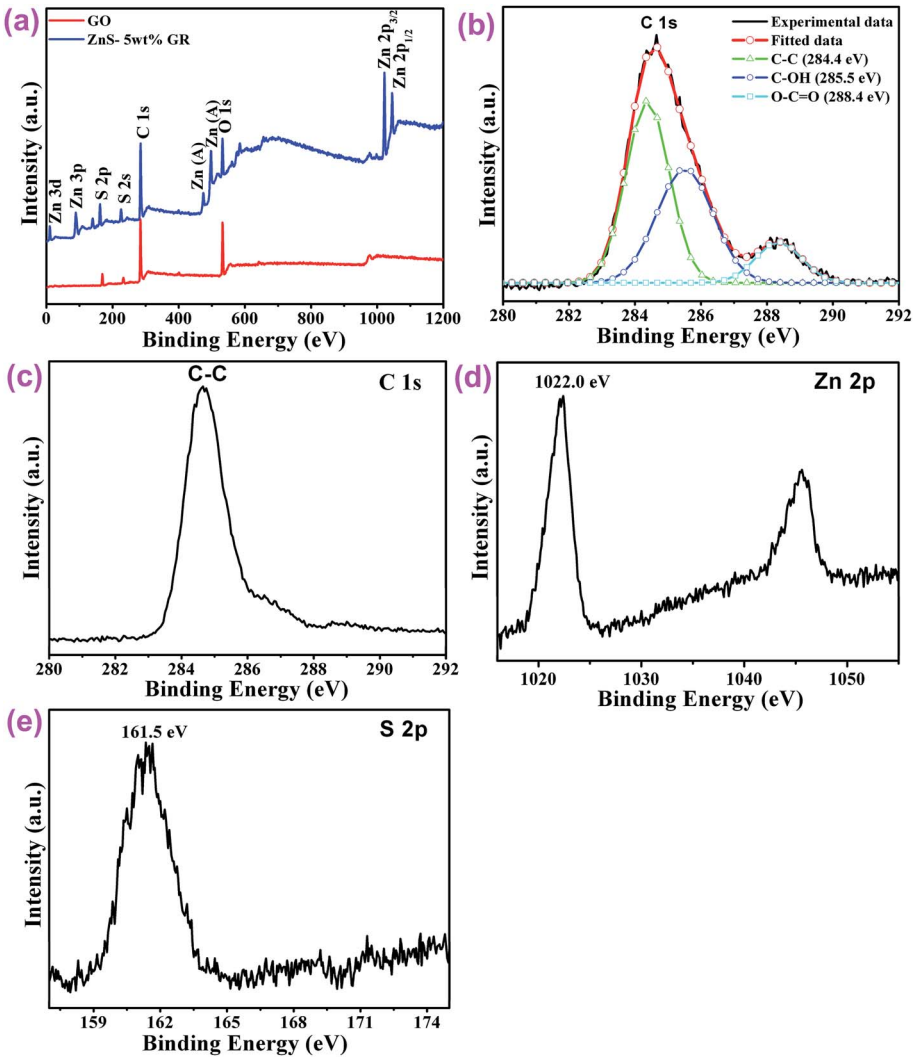

Fig. 6 (a) XPS survey spectrum of GO (red line) and ZnS–5 wt% GR nanocomposites (blue line); (b) and (c) high-resolution binding energy spectrum of C 1s for GO and ZnS–5 wt% GR nanocomposites; (d) and (e) high-resolution binding energy spectra of Zn 2p and S 2p for ZnS–5 wt% GR nanocomposites.

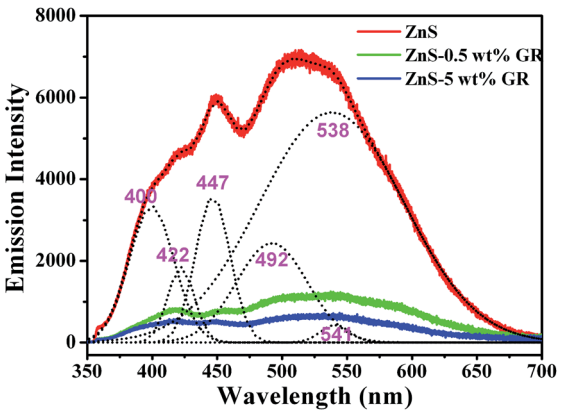

Fig. 7 Room temperature PL spectra of ZnS (red line), ZnS–0.5 wt% GR (green line) and ZnS–5 wt% GR (blue line) nanocomposites.

lattice defects,[47] 422 and 447 nm to the sulfur vacancy and surface states,[48,49] 492 nm to the self-activated defect centers formed by the zinc vacancy inside the lattice,[50] 538 and 541 nm to the sulfur species on the surface of ZnS NWs.[51] The PL intensity of ZnS–0.5 wt% GR (green line) and ZnS–5 wt% GR (blue line) nanocomposites is 5.8 and 10.6 times lower than that of ZnS NWs, further proving the effective interfacial electron-transfer process between GR and ZnS NWs. Since that GR is good electron acceptor and the excited ZnS NWs is good electron donor, the interaction between GR and ZnS NWs would lead to an increased transfer of the photogenerated electrons from ZnS NWs to GR[52] and reduce electron–hole pair recombination effectively.

The photocatalytic activity of ZnS NWs and ZnS–GR nanocomposites was evaluated by the degradation of organic dye MB under UV light irradiation. Fig. 8a shows the concentration changes of MB (C/C_0) during photodegradation as a function of UV light irradiation time, where C_0 and C are its initial

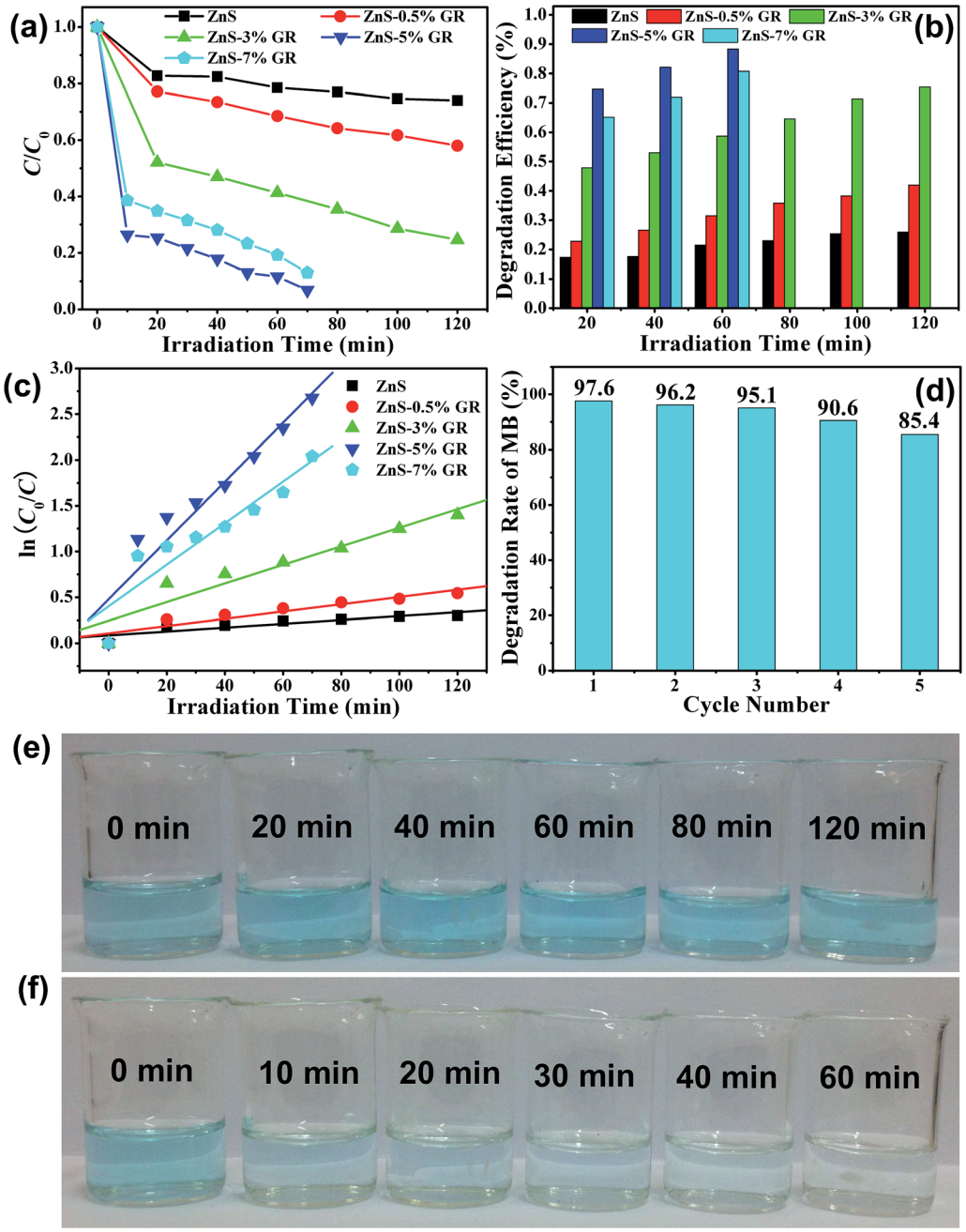

Fig. 8 (a) Photocatalytic degradation of MB under the irradiation of UV light with ZnS and ZnS–GR nanocomposites; (b) degradation efficiency of ZnS and ZnS–GR nanocomposites on the photodegradation of MB as a function of time; (c) plot of $\ln(C_0/C)$ as a function of UV irradiation time for the photocatalysis of MB solution containing ZnS and ZnS–GR nanocomposites; (d) reusability of the ZnS–5 wt% GR nanocomposite in the UV light degradation of MB solution. (e) and (f) the color variations of the MB solution for the ZnS and ZnS–5 wt% nanocomposites as the photocatalysts under the irradiation of UV light.

concentration and the concentration of MB after UV irradiation, respectively. In the 2 h of UV irradiation, the ZnS–GR nanocomposites show a remarkable enhancement in the photodegradation of MB compared with the ZnS NWs (Fig. 8a). After irradiation for 1 h, the degradation efficiency (Fig. 8b) is 21.69% for ZnS NWs, 31.52% for ZnS–0.5 wt% GR, 58.69% for ZnS–3 wt% GR, 88.33% for ZnS–5 wt% GR and 80.74% for ZnS–7 wt% GR, indicating the superior photocatalytic property of the ZnS–5 wt% GR nanocomposites. Seen from the image in Fig. 8f, almost all of the initial MB dyes are decomposed by ZnS–5 wt% GR nanocomposites after irradiation for 60 min, however, a great mass of MB still remain in the solution of ZnS NWs (Fig. 8e). The degradation kinetic of MB under UV light irradiation was also investigated by plotting the relationship between $\ln(C_0/C)$ and irradiation time (Fig. 8c). It can be seen that the curves of $\ln(C_0/C)$ *versus* irradiation time show linear lines, indicating a rather good correlation to first-order kinetics.[28] The determined k value for ZnS NWs, ZnS–0.5 wt% GR, ZnS–3 wt% GR, ZnS–5

wt% GR and ZnS–7 wt% GR is 2.1 × 10^{-3} min^{-1}, 3.9 × 10^{-3} min^{-1}, 10.1 × 10^{-3} min^{-1}, 32.1 × 10^{-3} min^{-1} and 22.7 × 10^{-3} min^{-1}, respectively. The photocatalytic activity of ZnS–5 wt% GR nanocomposites is about 16 times higher than that of ZnS NWs. The mechanism of the highly enhanced photocatalytic property for the ZnS–GR nanocomposites is investigated as follows. Under UV light irradiation, ZnS NWs are excited to generate electrons and holes. The separated electrons would subsequently react with water and oxygen to generate hydroxyl and superoxide radicals, the separated holes would directly react with MB or react with water to generate hydroxyl radicals.[24] The introduction of GR with high charge mobility[9,53] can act as good electron collector and transporter to restrain the electron–hole recombination and lengthen the lifetime of the photogenerated charge carriers from the ZnS NWs, thus leading to the higher photocatalytic efficiency of the ZnS–GR nanocomposites. Furthermore, GR with high surface area can offer more opportunities for the adsorption of the MB molecules on the surface of catalysts during the photodegradation reaction. However, the photocatalytic activity decreases at the GR content of 7%, which is probably due to the "shielding effect" caused by extra free GR.[54]

Reusability is also important for the practical application of photocatalysts. The durability of the catalyst for the degradation of MB under UV light irradiation was studied. Following a simple step of washing with water, the recycled photocatalyst was reused and the results of the photocatalyst degradation rate of MB are shown in Fig. 8d. The ZnS–5 wt% GR nanocomposites does not exhibit a significant loss of activity after five cycles of the degradation reaction, which indicates the stable structure of the ZnS–5 wt% GR nanocomposites throughout the photocatalytic process.

Conclusions

In this paper, the ZnS–GR nanocomposites were fabricated successfully by the electrostatic self-assembly method. The photocatalytic activity of ZnS NWs and ZnS–GR nanocomposites was evaluated by the degradation of organic dye MB under UV light irradiation. It was found that ZnS–5 wt% GR nanocomposites had the highest photocatalytic activity and the kinetic rate constant of the ZnS–5 wt % GR nanocomposites was about 16 times higher than that of the ZnS NWs. The mechanism of the highly enhanced photocatalytic property was attributed to the efficient separation of the photogenerated electron–hole pairs and the high specific surface area of graphene. Therefore, combining the good properties of 2D GR and 1D ZnS NWs would open up a promising way to develop novel and highly efficient GR-based heterostructure photocatalysts.

Acknowledgements

This work was financially supported by the National Programs for High Technology Research and Development of China (863) (Item no. 2013AA032202), the National Natural Science Foundation of China (grant no. 61008051, 61178074, 11204104, 11254001, 61378085, 61308095).

References

1 Q. J. Xiang, J. G. Yu and M. Jaroniec, *Chem. Soc. Rev.*, 2012, **41**, 782.
2 S. D. Zhuang, X. Y. Xu, B. Feng, J. G. Hu, Y. R. Pang, G. Zhou, L. Tong and Y. X. Zhou, *ACS Appl. Mater. Interfaces*, 2014, **6**, 613.
3 S. Q. Liu, M. Q. Yang and Y. J. Xu, *J. Mater. Chem.*, 2014, **2**, 430.
4 N. Zhang, Y. H. Zhang and Y. J. Xu, *Nanoscale*, 2012, **4**, 5792.
5 M. Q. Yang and Y. J. Xu, *Phys. Chem. Chem. Phys.*, 2013, **15**, 19102.
6 N. Zhang, M. Q. Yang, Z. R. Tang and Y. J. Xu, *ACS Nano*, 2014, **8**, 623.
7 R. R. Nair, P. Blake, A. N. Grigorenko, K. S. Novoselov, T. J. Booth, T. Stauber, M. R. Peres and A. K. Geim, *Science*, 2008, **320**, 1308.
8 K. S. Novoselov, A. K. Geim, S. V. Morozov, D. Jiang, Y. Zhang, S. V. Dubonos, I. V. Grigorieva and A. A. Firsov, *Science*, 2004, **306**, 666.
9 S. Stankovich, D. A. Dikin, G. H. B. Dommett, K. M. Kohlhass, E. J. Zimney, E. A. Stach, R. D. Piner, S. T. Nguyen and R. S. Ruoff, *Nature*, 2006, **442**, 282.
10 Y. M. Dong, C. Y. Feng, P. P. Jiang, G. L. Wang, K. Li and H. Y. Miao, *RSC Adv.*, 2014, **4**, 7340.
11 R. C. Pawar and C. S. Lee, *Appl. Catal., B*, 2014, **144**, 57.
12 L. Huang, X. L. Wang, J. H. Yang, G. Liu, J. F. Han and C. Li, *J. Phys. Chem. C*, 2013, **117**, 11584.
13 H. R. Rajabi, O. Khani, M. Shamsipur and V. Vatanpour, *J. Hazard. Mater.*, 2013, **250**, 370.
14 X. Fang, T. Zhai, U. K. Gautam, L. Li, L. Wu, Y. Bando and D. Golberg, *Prog. Mater. Sci.*, 2011, **56**, 175.
15 J. S. Hu, L. L. Ren, Y. G. Guo and H. P. Liang, *Angew. Chem., Int. Ed.*, 2005, **44**, 1269.
16 S. Bai, X. P. Shen, G. X. Zhu, H. Zhou, H. Xu, G. H. Fu and Z. F. Ye, *Eur. J. Inorg. Chem.*, 2013, **2**, 256.
17 X. L. Yu, G. J. Zhang, H. B. Cao, X. Q. An, Y. Wang, Z. J. Shu, X. L. An and F. Hua, *New J. Chem.*, 2012, **36**, 2593.
18 Y. H. Zhang, N. Zhang, Z. R. Tang and Y. J. Xu, *ACS Nano*, 2012, **6**, 9777.
19 J. Zhang, J. Yu, M. Jaroniec and J. R. Gong, *Nano Lett.*, 2012, **12**, 4584.
20 Q. Li, B. D. Guo, J. G. Yu, J. R. Ran, B. H. Zhang, H. J. Yan and J. R. Gong, *J. Am. Chem. Soc.*, 2011, **133**, 10878.
21 H. Li, C. Cheng, X. Li, J. Liu, C. Guan, Y. Y. Tay and H. J. Fan, *J. Phys. Chem. C*, 2011, **116**, 3802.
22 Z. Chen, N. Zhang and Y. J. Xu, *CrystEngComm*, 2013, **15**, 3022.
23 S. Liu, Z. Chen, N. Zhang, Z. R. Tang and Y. J. Xu, *J. Phys. Chem. C*, 2013, **117**, 8251.
24 Y. J. Wang, F. M. Wang and J. He, *Nanoscale*, 2013, **5**, 11291.
25 S. Liu, N. Zhang, Z. R. Tang and X. J. Xu, *ACS Appl. Mater. Interfaces*, 2012, **4**, 6378.
26 Z. R. Tang, Y. Zhang and X. J. Xu, *RSC Adv.*, 2011, **1**, 1772.
27 S. Khanchandin, S. Kundu, A. Patra and A. K. Ganguli, *J. Phys. Chem. C*, 2013, **117**, 5558.

28 L. Jia, D. H. Wang, Y. X. Huang, A. W. Xu and H. Q. Yu, *J. Phys. Chem. C*, 2011, **115**, 11466.
29 J. Wu, X. Shen, L. Jiang, K. Wang and K. Chen, *Appl. Surf. Sci.*, 2010, **256**, 2826.
30 H. Bai, Y. Xu, L. Zhao, C. Li and G. Shi, *Chem. Commun.*, 2009, **13**, 1667.
31 H. K. Jeong, Y. P. Lee, R. J. Lahaye, M. H. Park, K. H. An and I. J. Kim, *J. Am. Chem. Soc.*, 2008, **130**, 1362.
32 J. Y. Lee, D. S. Kim and J. Park, *Chem. Mater.*, 2007, **19**, 4663.
33 Y. Wang, R. Shi, J. Lin and Y. Zhu, *Appl. Catal., B*, 2010, **100**, 179.
34 T. Xu, L. Zhang, H. Cheng and Y. Zhu, *Appl. Catal., B*, 2011, **101**, 382.
35 Y. Zhang, Z. R. Tang, X. Fu and Y. J. Xu, *ACS Nano*, 2011, **5**, 7426.
36 Y. T. Liang, B. K. Vijayan, K. A. Gray and M. C. M. Hersam, *Nano Lett.*, 2011, **11**, 2865.
37 S. G. Pan and X. H. Liu, *J. Solid State Chem.*, 2012, **191**, 51.
38 Y. Feng, N. N. Feng, G. Y. Zhang and G. X. Du, *CrystEngComm*, 2014, **16**, 214.
39 L. H. Yu, H. Ruan, Y. Zheng and D. Z. Li, *Nanotechnology*, 2013, **24**, 375601.
40 Y. Feng, N. N. Feng, Y. Z. Wei and G. Y. Zhang, *RSC Adv.*, 2014, **4**, 7933.
41 B. Zeng, X. H. Chen, C. S. Chen, X. T. Ning and W. N. Deng, *J. Alloys Compd.*, 2014, **582**, 774.
42 H. T. Hu, X. B. Wang, F. M. Liu, J. C. Wang and C. H. Xu, *Synth. Met.*, 2011, **161**, 404.
43 J. H. Wang, S. Liang, L. Ma, S. J. Ding, X. F. Yu, L. Zhou and Q. Q. Wang, *CrystEngComm*, 2014, **16**, 399.
44 P. Wang, T. F. Jiang, C. Z. Zhu, Y. M. Zhai, D. J. Wang and S. J. Dong, *Nano Res.*, 2010, **3**, 794.
45 G. Deroubaix and P. Marcus, *Surf. Interface Anal.*, 1992, **18**, 39.
46 K. Laajalehto, I. Kartio and P. Nowak, *Appl. Surf. Sci.*, 1994, **81**, 11.
47 P. Hu, Y. Liu, L. Fu, L. Cao and D. Zhu, *J. Phys. Chem. B*, 2004, **108**, 936.
48 Y. Li, X. Li, C. Yang and Y. Li, *J. Phys. Chem. B*, 2004, **108**, 16002.
49 S. Kar, S. Biswas and S. Chaudhuri, *Nanotechnology*, 2005, **16**, 3074.
50 S. Biswas, S. Kar and S. Chaudhuri, *J. Phys. Chem. B*, 2005, **109**, 17526.
51 Z. Li, B. Liu, X. Li, S. Yu, L. Wang, Y. Hou, Y. Zou, M. Yao, Q. Li, B. Zou, T. Cui, G. Zou, G. Wang and Y. Liu, *Nanotechnology*, 2007, **18**, 255602.
52 Y. Yang and T. X. Liu, *Appl. Surf. Sci.*, 2011, **257**, 8950.
53 K. S. Novoselov, A. K. Geim, S. V. Morozov, D. Jiang, M. I. Katsnelson, I. V. Grigorieva, S. V. Dubonos and A. A. Firsov, *Nature*, 2005, **438**, 197.
54 J. Yu, T. Ma and S. Liu, *Phys. Chem. Chem. Phys.*, 2011, **13**, 3491.